Stresses and intermediate frequencies of strong earthquake acceleration*

M. D. Trifunac

University of Southern California, Civil Engineering Department,
Los Angeles, California, USA

The peak of smooth Fourier amplitude spectra, $(FS(T))_{max}$, of strong motion acceleration recorded in California is modeled *via* dimensional analysis. In this model, the spectrum amplitudes are proportional to (1) $\bar{\sigma}$ – the root-mean-square (r.m.s.) amplitude of the peak stresses on the fault surface in the areas of high stress concentration (asperities), and (2) $(\log_{10} N)^{1/2}$, where N is the number of contributing (sampled) asperities. The results imply simple, one asperity, earthquake events for $M \lesssim 5$, and multiple asperity events for $M \gtrsim 5$ ($N \sim 10$ near $M = 7$ and $N \sim 100$ for $M \sim 8$). The r.m.s. value of the peak stress drop on the fault, $\bar{\sigma}$, appears to increase with magnitude for $M \lesssim 6$, and then it levels off near 100 bars, for $M \gtrsim 6$. For $M > 6$, $(FS(T))_{max}$ continues to grow with magnitude, because of the larger number of asperities from which the sample is taken ($N \sim 100$ for $M = 8$), not because of increasing $\bar{\sigma}$.

Keywords: Strong earthquake acceleration, earthquake stress.

Introduction

The Fourier amplitude spectra of strong earthquake ground acceleration, $FS(T)$, could be viewed and studied in three frequency ranges: (1) long periods (frequencies $f = 1/T \leq f_1 \sim v/L$, where v – dislocation velocity, L - fault length, Fig. 1; Trifunac, 1993), (2) high frequencies ($f > f_H = Q\beta/5\Delta$, where Q – quality factor, β – shear wave velocity and Δ – hypocentral distance; Trifunac, 1994a) and (3) intermediate frequencies ($f_1 < f \leq f_H$). For long periods, in the near-field, $FS(T)$ is determined by the average value of the permanent

---

fault offset, $\bar{u}$, and by the fault geometry (fault width W and length L), and in the far-field by the seismic moment M_o. For intermediate frequencies, $FS(T)$ is determined by the stresses on the fault (Brune, 1970). At high frequencies, $FS(T)$ is still determined by the stresses on the fault, but its final amplitudes are governed by the attenuation and scattering properties of the geological environment, around the source, and between the source an the recording station.

There have been many studies of Fourier amplitude spectra of strong motion acceleration since 1970's (reviewed by Anderson, 1991). Most of these are seismological studies which have focused on far-field body wave spectra. For earthquake resistant design, however, it is necessary to represent the complete strong motion signal close to the fault plane, including near-field, intermediate field and far-field body and surface waves in the representation of the ground motion (Trifunac, 1974). While much can be learned about the nature of the problem from seismological (theoretical and observational) studies of body and surface wave spectra, strong ground motion for engineering applications is best represented by direct scaling models, obtained by regression analyses of recorded accelerograms, which represent the complete strong motion signal (Trifunac, 1995a,b). Empirical scaling models can predict the average trends of $FS(T)$ of strong motion amplitudes near the source (hypocentral distance $\Delta \lesssim 100\,\text{km}$), for frequencies $\sim 0.1 < f < 25 <$ Hz. The proximity of the recording stations to the source (implying short and relatively simple propagation path), high frequency characteristics of strong motion accelerographs and high quality data processing, all contribute to the accuracy and completeness of information contained in strong motion accelerograms.

This paper employs dimensional analysis to examine the Fourier amplitude spectra of the complete strong motion signal in the intermediate frequency range ($f_1 < f < f_H$), in relation to selected parameters of the earthquake source (*e.g.*, earthquake magnitude, M, seismic moment, M_o, average dislocation amplitude on the fault surface, $\bar{u}$, stress drop, σ). The functional forms used in this dimensional analysis will follow from elementary models of the earthquake source, and are calibrated *via* empirical scaling models of recorded strong motion (Trifunac 1989a, b; Trifunac and Lee, 1989). The purpose of the study is to use the wealth of information contained in the Fourier spectrum of recorded motion (*via* empirical scaling models) to delineate the nature of the functional relationships between various quantities describing the physical processes of the earthquake source, and especially the stress drop as function of the earthquake magnitude. Finally, an implication of the earthquake source model, resulting from this study, for frequency of occurrence versus magnitude relationships for a region (important for probabilistic earthquake hazard assessment) is discussed.

Empirical scaling models for *FS*(*T*)

Models for empirical scaling the Fourier amplitude spectra of strong motion acceleration, *FS*(*T*), have the form

$$\log_{10} FS(T) = M + Att(\Delta, M, T) + b_1(T)M + b_2(T)h + b_3(T)\mathrm{v} + b_4(T)h\mathrm{v} +$$
$$+ b_5(T) + b_6(T)M^2 + b_7^{(1)}(T)S_L^{(1)} + b_7^{(2)}(T)S_L^{(2)}, \tag{1}$$

where M is the earthquake magnitude (Richter, 1958; Trifunac, 1991), $b_1(T)$ through $b_7^{(2)}(T)$ are scaling coefficient functions of period T, and $Att(\Delta, M, T)$ is the frequency dependent attenuation function (Trifunac and Lee, 1990)

$$Att(\Delta, M, T) = \begin{cases} A_o(T)\log_{10} \Delta & R \le R_o \\ A_o(T)\log_{10} \Delta_o - (R - R_o)/200, & R > R_o \end{cases} \tag{2}$$

In eq. (2), R is the epicentral distance, H is the focal depth, Δ is the »representative« source-to-station distance,

$$\Delta = S \ln \left[\frac{R^2 + H^2 + S^2}{R^2 + H^2 + S_o^2} \right]^{-\frac{1}{2}} \tag{3}$$

and Δ_o is the value of Δ when $R = R_o$ (all of these are in km).

The attenuation $Att(\Delta, M, T)$ depends on magnitude implicitly, through S, which is the linearized estimate of the »source dimension«

$$S = 0.2 + 8.51(M - 3), \quad \text{for } M > 3. \tag{4}$$

S_o in eq. (3) is the coherence radius of the source, approximated by $S_o \sim \beta T / 2$, where β is the shear wave velocity in the source region. When $S/R \to 0$ and $S/R_o \to 0$ (*i.e.* large R or small S and S_o), $\Delta \to (H^2 + R^2)^{1/2}$ = hypocentral distance.

The function $A_o(T)$, in the right hand side of eq. (2), is represented by a parabola of T between 0.04 s and about 1 s. It increases from ≈ -2 at $T = 0.04$ s to ≈ -0.7 at $T = 1$ s, and remains constant for $T > 1$ s. R_o is the transition distance (about 150 km for $T < 0.05$, and ~ 50 km for $T > 1$ s) beyond which the attenuation function has slope of 1/200.

In eq. (1), h represents the thickness of the sedimentary layer (in km) at the site. The parameter v equals 0 for horizontal motion and 1 for the vertical motion. The term $b_4(T)h\mathrm{v}$ models progressively steeper incidence of body waves for soft and deeper sedimentary sites, $b_5(T)M^2$ models the saturation of strong motion amplitudes versus M, for $M < M_{\max} = -(1 + b_1(T))/(2b_6(T))$.

The last two terms of eq. (1) contain indicator variables $S_L^{(1)}$ and $S_L^{(2)}$ defined by

$$S_L^{(1)} = \begin{cases} 1 \text{ if } s_L = 1 \text{ (stiff soil)} \\ 0 \text{ otherwise} \end{cases} \quad \text{and} \quad S_L^{(2)} = \begin{cases} 1 \text{ if } s_L = 2 \text{ (deep soil)} \\ 0 \text{ otherwise} \end{cases} \quad (5)$$

where s_L is the local soil parameter (s_L = 0, 1 and 2 represents »rock«, stiff soil and deep soil sites; Trifunac, 1990). Sites with soft to medium clays, with strata of sands and gravels, are not common in the Western United States and are not considered in the regression model.

Let $\widehat{FS}(T)$ represent the Fourier amplitude spectrum estimated from eq. (1) and $FS(T)$ the spectrum computed from recorded accelerograms. The residues, $\varepsilon(T)$, defined as

$$\varepsilon(T) = \log_{10} FS(T) - \log_{10} \widehat{FS}(T), \quad (6)$$

can be described by a normal distribution function, with mean $\mu(T)$ and standard deviation $\sigma(T)$. Then the probability that $\log_{10} FS(T) - \log_{10} \widehat{FS}(T) \le \varepsilon(T)$ is

$$p(\varepsilon, T) = \frac{1}{\sigma(T)\sqrt{2\pi}} \int_{-\infty}^{\varepsilon(T)} \exp\left[-\frac{1}{2}\left(\frac{x - \mu(T)}{\sigma(T)} \right)^2 \right] dx \quad (7)$$

Table 1 gives $b_1(T)$ through $b_7^{(2)}(T)$, M_{min}, M_{max}, $\mu(T)$ and $\sigma(T)$ at 12 periods $T(1) = 0.04$ through $T(12) = 14$ s.

Table 1.

$$\log_{10} FS(T) = M_< + Att(\Delta, M, T) + b_1(T)M_{<>} + b_2(T)h + b_3(T)\text{v} + b_4(T)h\text{v} +$$
$$+ b_5(T) + b_6(T)M_{<>}^2 + b_7^{(1)}(T)S_L^{(1)} + b_7^{(2)}(T)S_L^{(2)}$$

$N =$	1	2	3	4	5	6	7	8	9	10	11	12
Period T (s) =	0.040	0.065	0.11	0.19	0.34	0.50	0.90	1.60	2.80	4.40	7.50	14.0
Coefficients:												
$b_1(T)$	0.652	0.667	0.819	0.962	0.977	0.927	0.854	0.876	0.940	0.856	0.382	−0.707
$b_2(T)$	0.067	0.063	0.056	0.047	0.040	0.039	0.049	0.067	0.084	0.087	0.069	0.020
$b_3(T)$	0.127	0.091	−0.012	−0.155	−0.272	−0.292	−0.233	−0.152	−0.122	−0.126	−0.132	−0.131
$b_4(T)$	0.006	−0.002	−0.015	−0.030	−0.041	−0.047	−0.051	−0.048	−0.040	−0.033	−0.030	−0.034
$b_5(T)$	−3.921	−3.876	−4.151	−4.532	−4.809	−4.924	−5.151	−5.568	−5.881	−5.529	−3.791	−0.019
$b_6(T)$	−0.095	−0.098	−0.114	−0.127	−0.128	−0.123	−0.112	−0.110	−0.113	−0.110	−0.080	−0.006
$b_7^{(1)}(T)$	−0.314	−0.282	−0.219	−0.120	−0.008	0.052	0.120	0.161	0.161	0.127	0.065	−0.002
$b_7^{(2)}(T)$	−0.264	−0.260	−0.151	−0.012	0.069	0.144	0.169	0.152	0.103	0.004	−0.144	
M_{min}	3.429	3.389	3.604	3.780	3.810	3.773	3.814	3.991	4.155	3.897	2.376	0.000
M_{max}	8.691	8.472	8.006	7.711	7.711	7.845	8.282	8.549	8.576	8.450	8.600	14.500
$\mu(T)$	−0.002	−0.002	−0.002	−0.001	−0.001	−0.001	−0.002	−0.001	0.002	0.003	0.001	−0.001
$\sigma(T)$	0.445	0.462	0.388	0.343	0.316	0.317	0.338	0.352	0.343	0.328	0.315	0.305

$M_< = \min(M, M_{max})$, $M_{<>} = \max(M_{min}, M_<)$

The first empirical scaling models of Fourier spectra of strong earthquake motion were developed in 1976 (Trifunac, 1976), and use the Richter's attenuation function (Richter, 1958). The first models which consider frequency dependent attenuation – $Att(\Delta, M, T)$ given by eq. (2) – were developed in 1985, but these did not consider explicitly dependence on the soil site parameter s_L (Trifunac and Lee, 1985). This dependence was included in the further generations of regression models (Trifunac and Lee, 1987; 1989). The thickness of sediments, h, is often not known at the recording stations or at sites where the empirical scaling models for $FS(T)$ will be applied. An alternative simple way of defining the site geology has been *via* the geologic site condition parameter s (= 0, 1 and 2 for sediments, intermediate sites and rock). The resulting empirical models are almost identical to the one in eq. (1), except that the dependence on h is replaced by an equivalent dependence on s.

This paper uses the following four empirical scaling models:

1. MAG-SITE (Trifunac and Lee, 1989)

2. MAG-DEPTH (Trifunac and Lee, 1989)

3. MAG-SITE-SOIL (Trifunac, 1989b)

4. MAG-DEPTH-SOIL (Trifunac, 1989a)

In what follows, these four models will be used simultaneously and will be referred to as the »group of four« recent scaling models (G4RM). In the above »MAG« implies scaling in terms of earthquake magnitude, »SITE« indicates use of the geological site parameters s = 0, 1 or 2, and »DEPTH« implies use of h as in eq. (1). »SOIL« indicates that the soil site parameter s_L (= 0, 1 and 2) is considered. Models 1 and 2 do not consider dependence on s_L.

Figure 1 shows $\log_{10} FS(T)$ versus frequency f = 1/T for magnitudes M = 4, 5, 6, 7 and 8, at epicentral distance R = 10 km, for source depth H = 0 km, and for 50 % probability of exceedance (*i.e.* $p(\varepsilon, T) = 0.5$, see eq. (7)). With decreasing magnitude and increasing source to station distance, the spectral amplitudes computed by eq. (1) are valid up to progressively shorter periods $(T(N_c) = 1/f_{C_0})$. This is caused by the recording and processing noise, whose spectral amplitudes are shown in Fig. 1 by the shaded zone (increasing from about 0.1 cm/s for $f \sim$ 10 Hz to about 3 cm/s near f = 0.1 Hz (Lee and Trifunac, 1990; Lee et al. 1982). At the higher frequency end, the spectra are defined only up to 25 Hz; this limit is chosen more for convenience in data processing than for poor signal to noise ratio. Also, at high frequencies, the spectral amplitudes recorded by the strong motion accelerographs are smaller than indicated in Fig. 1, because most strong motion transducers which contributed to the strong motion database used for the statistical regression had natural frequencies between 14 Hz and 25 Hz (Trifunac and Hudson, 1970; Trifunac, 1971, 1972c; Lee et al., 1982). While the algorithms for correction of instrument response and for reconstruction of ground motion can be extended to apply for frequencies higher than 25 Hz, so far it has not been necessary to
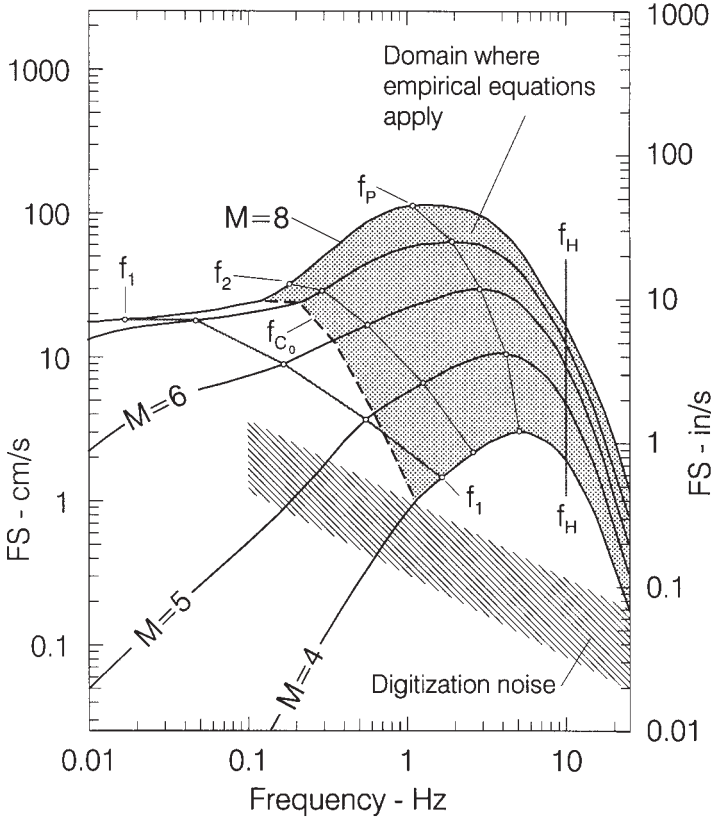
Figure 1. Fourier amplitude spectra, versus frequency (Hz) for probability of exceedance equal to 0.5, for M = 4, 5, 6, 7 and 8, at epicentral distance R = 10 km and for the source at depth H = 0 km. Outside the shaded region, between f_{C_o} =1/$T(N_c)$ and f = 25 Hz, where equation (1) is valid, the spectral amplitudes can be extrapolated as it is suggested in Trifunac (1993). The corner frequencies f_1, f_2, the cut off frequencies f_{C_o}, and f_P and f_H are defined in the text. The processing and digitization noise amplitudes are shown by the rectangular shaded zone.

preserve the digitized data at sampling rate higher than 50 points/s (Lee and Trifunac, 1990). In Fig. 1, the shaded area shows the region where the empirical eq. (1) is valid. For uniformity, all G4RM empirical equations are defined for 12 periods $T(N)$, N = 1, ..., 12 (Table 1), but can be used only for $N \leq N_c$. Table 2 shows the cut-off periods, $T(N_c)$, $(T(N_c) = 1/f_{C_o})$, versus magnitude.

In what follows, the spectral amplitudes for intermediate frequencies near the peak amplitudes of $FS(T)$ will be studied (at f_p in Fig. 1). Also, all spectra and analyses will be based on the estimates of strong ground motion at basement rock (s = 2, or h = 0) and on »rock« soil site (s_L = 0). This will eliminate complications introduced by the local site conditions (Trifunac,

1990) and will allow more direct comparison with seismological studies and observations. Finally, the results of eq. (1) for horizontal motions only (v = 0), will be presented.

Table 2. Cut-off periods T(N$_c$) versus magnitude

M	T(N$_c$)	N$_c$
3	0.90	7
4	0.90	7
5	1.60	8
6	2.80	9
7	4.40	10
8	7.50	11

Long period extension

In the near-field, $FS(T)$ may be extrapolated for periods longer than $T(N_c)$ (Table 2) by the function (Trifunac, 1993)

$$FS_{NF}(T) = \frac{\frac{2\pi}{T}\overline{d}}{\left[\left(\frac{2\pi\tau}{T}\right)^2 + 1\right]^{1/2}} \tag{8}$$

where $\overline{d}$ is the average permanent ground displacement on the surface, at the fault, and τ is the characteristic source time ($\tau = 1/f_1$). The latter can be approximated by

$$\tau \sim \left(\frac{L}{v} + \frac{W}{6}\right) \tag{9}$$

where v is the dislocation velocity (~ 2.2 km/s), and L and W are the rupture length and width. At $T = T(N_c)$, the amplitude of the extension function $FS_{NF}(T)$ has to be equal to amplitude of the empirical model $FS(T)$. This condition can be used to evaluate the average permanent ground displacement $\overline{d}$ as function of the Fourier amplitude spectrum of recorded acceleration. The average dislocation amplitude on the ruptured area is $\overline{u} = 2\overline{d}$. Consequently, the condition $FS_{NF}(T) = FS(T)$ at $T = T(N_c)$ results in estimates of $\overline{u}$ versus earthquake magnitude, which will be used throughout this paper.

In the far-field, $FS(T)$ can be extrapolated for periods longer than $T(N_c)$ by the function (Trifunac, 1993)

$$FS_{FF}(T) = C_s \left(\frac{2\pi}{T}\right)^2 \frac{1}{\left[1 + \left(\dfrac{W}{22T}\right)^2\right]^{1/2}} \cdot \frac{1}{1 + \dfrac{\tau}{T}} \tag{10}$$

where C_s is a parameter determined from the condition that $FS_{FF}(T) = FS(T)$ at $T = T(N_c)$.

In eqs. (9) and (10), the fault length, L, and width, W, are defined by

$$L = a\,10^{bM} \tag{11}$$

and

$$W = c\,10^{dM} \tag{12a}$$

or

$$W = e + fM \tag{12b}$$

where the constants a through f for the G4RM are specified in Table 3. These four models have been chosen to illustrate variations in the definitions of W and L, but all fit the data and many other constraints on the source parameters (Trifunac, 1994b). In the following, these models will be referred to as the »four extrapolation models«. Table 4 summarizes selected source parameters which are associated with these four extrapolation models. In this table M_0 is the seismic moment, $f_2 = v/W$ and $A = WL$.

Stress characteristics of the source

In this analysis, the »stress drop« will be used *via* dimensional analysis as a scaling parameter which governs the amplitudes of Fourier amplitude

Table 3. *Coefficients* a *and* b *in* L = a $\times 10^{bM}$ *and* c *and* d *in* W = c $\times 10^{dM}$

	Fault length L (km)			Fault width W (km)		
Model	a	b	conditions			
1	0.0936	0.514	$M > 4.77^*$	$W = \begin{cases} -377 + 13.47M \\ 0.131M \end{cases}$		$M > 3.1^*$ $M < 3.1$
				c	d	
2	0.0133	0.500		0.1 $W = L$	0.25 for	$M > 3.5^*$ $M < 3.5$
3	0.00931	0.515		0.132 $W = L$	0.245 for	$M > 4.25^*$ $M < 4.25$
4	0.00931	0.515		0.132 0.0145	0.245 0.419	$M > 5.5^*$ $M < 5.5$

*in the text these magnitudes are designated by M_*

Table 4. Selected source parameters of the »four extrapolation models«

	M	Model 1		Model 2		Model 3		Model 4	
$\log_{10} \overline{u}$	3	−0.95	−0.71	−0.92	−0.68	−1.00	0.76	−1.02	−0.78
(cm)	4	0.60	0.75	0.49	0.64	0.43	0.58	0.39	0.54
	5	1.44	1.49	1.46	1.51	1.41	1.46	1.40	1.45
	6	2.36	2.42	2.41	2.46	2.36	2.41	2.37	2.41
	7	3.05	3.18	3.11	3.23	3.06	3.19	3.05	3.19
	8	3.52	3.71	3.57	3.76	3.54	3.72	3.54	3.72
$\log_{10} A$	3	−0.81		−0.75		−0.95		−1.07	
(km^2)	4	0.42		0.12		0.06		−0.13	
	5	1.01		0.87		0.89		0.80	
	6	1.69		1.63		1.65		1.65	
	7	2.32		2.37		2.41		2.41	
	8	2.93		3.12		3.17		3.17	
$\log_{10} M_o$	3	20.54	20.66	20.56	20.67	20.51	20.62	20.50	20.61
(dyn cm)	4	22.42	22.54	22.23	22.35	22.20	22.32	22.10	22.23
	5	23.38	23.43	23.33	23.38	23.32	23.37	23.29	23.34
	6	24.84	24.89	24.84	24.89	24.82	24.88	24.82	24.88
	7	26.26	26.39	26.30	26.43	26.29	26.42	26.29	26.42
	8	27.61	27.80	27.68	27.87	27.68	27.87	27.68	27.87
f_1 (Hz)	3	4.10		3.82		4.93		5.21	
	4	1.00		1.29		1.51		1.67	
	5	0.48		0.45		0.51		0.53	
	6	0.17		0.15		0.17		0.17	
	7	0.056		0.050		0.055		0.055	
	8	0.018		0.016		0.017		0.017	
f_2 (Hz)	3	5.60		5.22		6.47		8.40	
	4	1.36		2.20		2.06		3.20	
	5	0.74		1.24		0.99		1.22	
	6	0.51		0.70		0.56		0.57	
	7	0.39		0.39		0.32		0.32	
	8	0.31		0.22		0.18		0.18	

spectra of strong motion at intermediate frequencies (1 to 5 Hz). The stress $\sigma = \sigma_o - \sigma_f$ will be referred to as effective stress. It represents the difference between the stress on the fault before the earthquake, σ_o, and the frictional stress, σ_f, opposing the dislocation. For simplicity, it be will assumed that σ equals the stress drop.

Peak Amplitudes of FS(T)

For frequencies $1/T > f_c$ (corner frequency), the peak amplitude of smooth Fourier spectrum of strong motion acceleration is proportional to

$$FS(T)_{\max} \sim \sigma \beta / \mu \qquad (13)$$

where $FS(T)_{max}$ is the high frequency spectral asymptote in an ideal medium with no attenuation (Brune, 1970). For stations near the source, the corner frequency, f_c, depends on the wave type and on the source-to-site distance. It can be approximated by $f_c \sim \max[f_1, f_2]$, with $f_1 \sim [L/v + T_o]^{-1}$ and $f_2 \sim v/W$, where T_o is the dislocation rise time.

As the frequency increases, the attenuation and scattering diminish the spectral amplitudes approximately like $\exp[-(\pi f \Delta)/(Q\beta)]$. This attenuation becomes pronounced near $f_H = [(Q\beta)/(5\Delta)]$, and begins to dominate the shape of the spectral amplitudes for $f > f_H$ (Trifunac, 1973; 1994a, b). For small earthquakes (Fig. 1), f_c may be close to or higher than f_H, so that the constant plateau $\sigma\beta/\mu$ in eq. (13) may not be attained. In those instances, the peak spectral amplitudes will be smaller than $\sigma\beta/\mu$, and can serve only as a lower bound estimates of σ. The peaks of $FS(T)$ occur near $T = 0.2$ s ($f_p = 5$ Hz, Fig. 1) for $M = 4$ and move towards $T = 1$ s ($f_p = 1$ Hz) for $M = 8$.

The empirical scaling eq. (1) for the G4RM can be used to evaluate the peak amplitudes of $FS(T)$ for $\Delta = 0$. Taking $\beta \sim 3.5$ km/s and $\mu \sim 1.3 \times 10^{11}$ dyn/cm^2 gives $\sigma \sim [FS(T)]_{max}$ (in bars if $FS(T)$ is measured in in/s). In Fig. 2, this estimate of σ is compared with the results of several studies on stress drop in the same area and for some of the same earthquakes which contrib-
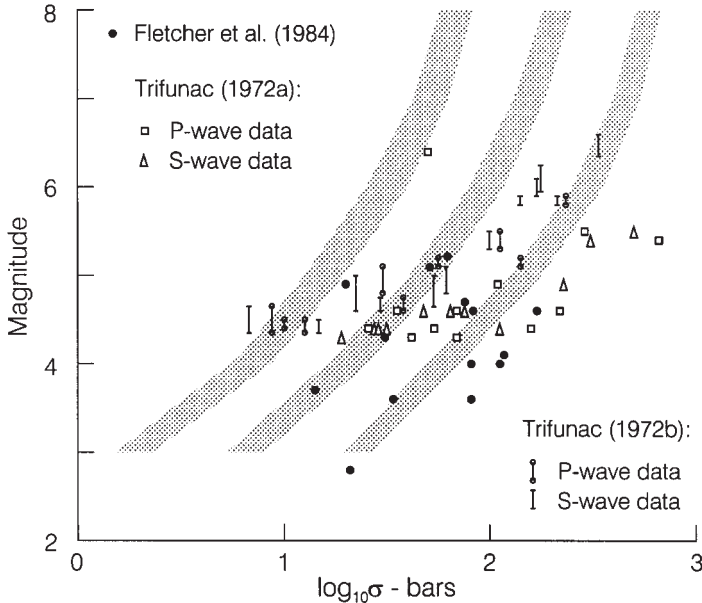

Figure 2. Estimates of stress drop versus magnitude, with examples from near source recordings. The three shaded zones represent the range of stresses for the G4RM and for probabilities of exceedance $p = 0.1, 0.5$ and 0.9.

uted to the strong motion database used to develop the G4RM. It is seen that the source mechanism studies suggest wide scatter of stress drop with respect to magnitude. The three shaded areas in Fig. 2, for $p = 0.1$, 0.5 and 0.9 have been computed from G4RM, for $3 < M < 8$.

Static stress drop

The average static stress drop, σ, can be computed from the average dislocation amplitude, $\bar{u}$, the source dimension, r and the rigidity of the surrounding rock, μ, as follows

$$\sigma = \frac{\bar{u}\,\mu}{C_0 r}. \qquad (14)$$

C_0 is given in Table 5 for several classical solutions, and r is defined by the geometry of the source. $\bar{u}$ is the average dislocation amplitude and can be computed from the condition that, in the near-field, $FS_{NF}(T) = FS(T)$ at $T = T(N_c)$, as discussed in the previous section. Smaller earthquakes, probably occur near stress concentrations on the fault associated with or caused by higher rigidity, μ, while the large events (say $M \geq 6$ and 7) result in large rupture areas, and are associated with average μ. It will be assumed here that for $M = 3, 4, 5, 6,$ and 7, one can take $\mu = (4, 3, 2, 1,$ and $1) \times 10^{11}$ dyn/cm^2. The fault dimension r can be approximated by W, which in turn can be computed from the empirical models in Table 3. The scaling constant C_0

$$C_{0=} \frac{\bar{u}\,\mu}{W\sigma} \qquad (15)$$

Table 5.

$$\bar{u} = C_0 \sigma r / \mu, \quad \bar{u} = 2\bar{d}$$

Type of faulting and fault geometry	C_0	r represents
Dip-slip displacement along an infinitely long narrow strip in a uniform shear field (Star, 1928)	$\dfrac{3\pi}{16}$	Fault width
Infinitely long vertical surface fault with strike slip displacement (Knopoff, 1958)	$\dfrac{\pi^{*}}{2}$ to $\dfrac{\pi^{**}}{4}$	Fault width
Circular fault plane in an infinite medium (Keilis-Borok, 1959)	$\dfrac{8}{7\pi}$	Diameter of circular dislocation (Fault width)

can be estimated empirically for the four extrapolation models (Fig. 3). It increases from ~0.3 to ~1.6 for magnitudes $3 < M < 7$. The average trend of C_0 is approximated by $C_0^* = 0.4, 0.5, 0.65, 0.85$ and 1.6 for $M = 3, 4, 5, 6$ and 7 (Trifunac, 1994b).

By substituting for $\bar{u}$ in terms of the seismic moment $M_o = \mu A \bar{u}$, and with $A = WL$, in eq. (14), it follows

$$\sigma = \frac{M_o}{C_0 L W^2}. \tag{16}$$

Assuming $\bar{u} \sim [(\sigma \beta) / \mu] T_o$ (Brune, 1970) and $v \sim \beta$ implies

$$\sigma \sim \frac{\mu \bar{u} f_2}{C_0^* \beta} \tag{17}$$
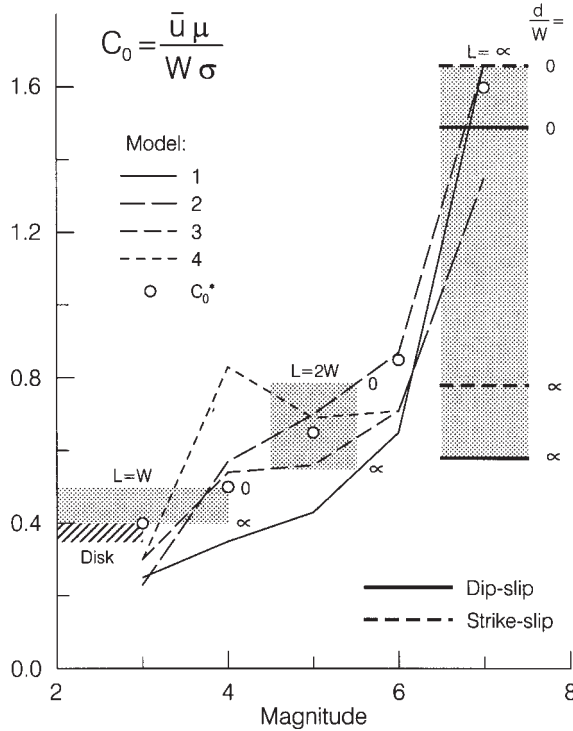
Figure 3. $C_0 = \bar{u} \mu / (W \sigma)$ versus magnitude for the four extrapolation Models 1 through 4. Shaded areas show the range of C_0 derived from analytical (disk) and numerical analyses of static displacements surrounding a rectangular fault (W = width, L = length) and at depth d ($d = 0$ for surface faults, $d = \infty$ for a fault in elastic full space). C_0 from theoretical solutions for infinitely long faults are shown with solid and dashed lines.

where $f_2 = v/W$ and T_o is the dislocation rise time for Haskell (1969) type dislocation.

Equations (14), (16) and (17) are not independent, but show how different combinations of source parameters can be used to evaluate σ. These parameters are derived from the long ($\overline{u}$ and M_o, L *via* f_1) and intermediate (W *via* f_2, T_o) period parts of empirical spectra, from the parameters which are based on the assumed extrapolated nature of the spectral amplitudes ($\overline{u}$, L), and parameters which can be estimated from strong motion data (M_o, W *via* f_2, T_o). Agreement of various estimates based on eqs (14), (16) and (17) can also serve as an internal consistency test for properly chosen scaling parameters.

If the average (representative) μ is known, the stress drop can be computed from the quantity σ/μ, which represents the »strain drop« during an earthquake. The strain drop is equal to $\overline{u}/(WC_0^*)$, and represents intermediate (W) and long period ($\overline{u}$) estimate. Figure 4 presents $\log_{10}[\overline{u}/(WC_0^*)]$ for the four extrapolation models, plotted versus $\log_{10}M_o$. It shows a well defined linear growth which can be represented by
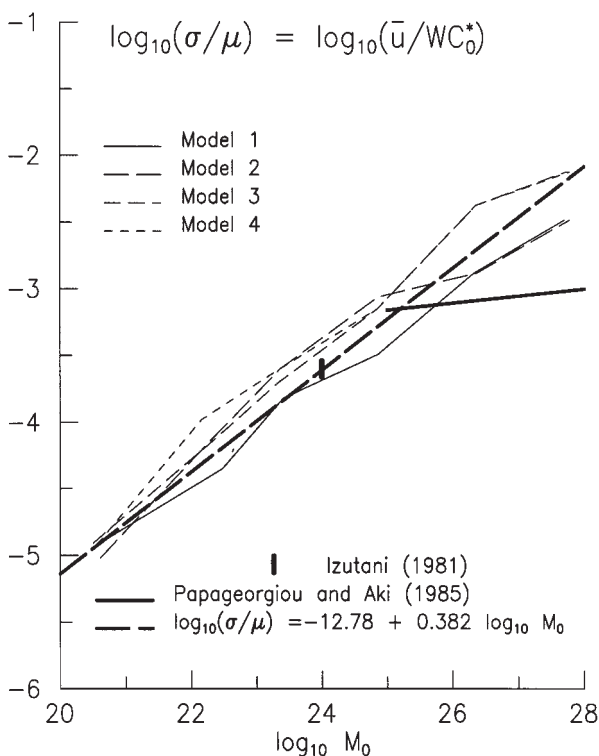
Figure 4. Strain drop, $\log_{10}(\sigma/\mu) = \log_{10}[u/(WC_0^*)]$ versus $\log_{10}M_o$.

$$\log_{10} \frac{\sigma}{\mu} = \log_{10} \frac{\overline{u}}{WC_0^*} = -12.78 + 0.382 \log_{10}M_o. \tag{18}$$

For comparison the results of Izutani (1981) and Papageorgiou and Aki (1985) are shown. The strain increases from $\sim 10^{-5}$ for $M = 3$ ($\log_{10}M_o \approx 20$) to $\sim 10^{-3}$ for $M = 7$ ($\log_{10}M_o \approx 27$).

It is reasonable to speculate that small earthquakes occur around high stress concentrations which are associated with »more rigid« geological environment, since in the inhomogeneous material more rigid components will tend to »attract« higher forces (stresses). For this reason, $\mu = (4, 3, 2, 1$ and $1)$ $\times 10^{11}$ dyn/cm^2 for analysis involving $M = 3, 4, 5, 6$ and 7 earthquakes has been used. This hypothesis can be »tested« by computing σ from $FS(T)_{max}$ and dividing the result by σ/μ from $\log_{10}(\sigma/\mu)$, computed from eq. (18), with the assumed relationship $\log_{10}M_o = 1.5M + 16$. Using average stress drop shown in Fig. 2 gives $\mu \sim (5, 4, 3, 2$ and $1) \times 10^{11}$ dyn/cm^2 for $M = 3, 4, 5, 6$ and 7.

Dynamic stress drop

Next we assume $\sigma \sim FS(T)_{max}$, and ignore the possible low-pass filtering effects (resulting in smaller values of σ) caused by Q, for small magnitude events, say $M \leq 4$. Then referring to Fig. 2, we explore observerd trends of σ.
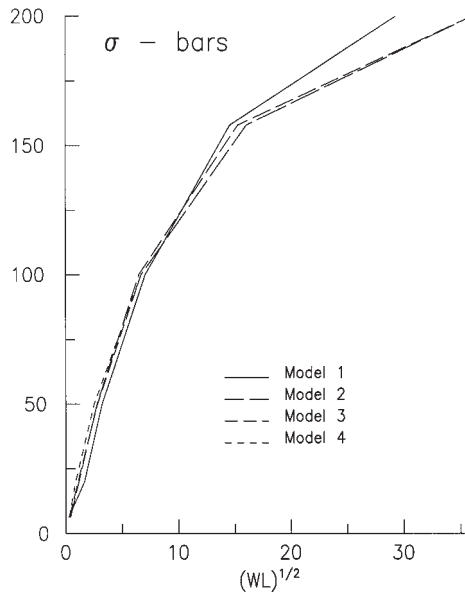

Figure 5. Stress drop versus characteristic fault dimension $(WL)^{1/2}$.

Joyner (1984) suggests that high frequency spectral acceleration should be proportional to $A^{1/2}$ for all earthquakes. To test this hypothesis, σ was plotted versus $(WL)^{1/2}$ for the four extrapolation models. The results are shown in Fig. 5. If σ can be estimated by $FS(T)_{\max}$ at $\Delta = 0$, and the four extrapolation models are representative, then this hypothesis by Joyner does not hold. As Fig. 5 shows, σ increases at a progressively slower rate as $(WL)^{1/2}$ increases. Thus σ is not proportional to a linear dimension of the source.

Scholz (1982) believes that $\bar{u} \sim L$ and that $\bar{u} \nsim W$ and presents alternatives to the common relations between σ and the fault width. Our analyses show that $\bar{u}$ does not depend linearly either on L or on W (Figs. 6 and 7). Plots of $\bar{u}$ versus L on a linear scale (so that small dislocation amplitudes are compressed near the origin) suggest that, for $M = 7$ and 8, $\bar{u} \sim \alpha L$, where $\alpha = 37.5$. However, most of the available strong motion data are for earthquakes with magnitudes $M < 7$, and, so, this cannot be taken as a reliable support for the hypothesis that $\bar{u} \sim L$. It is of interest to note that Scholz (1982) finds 10 to 15
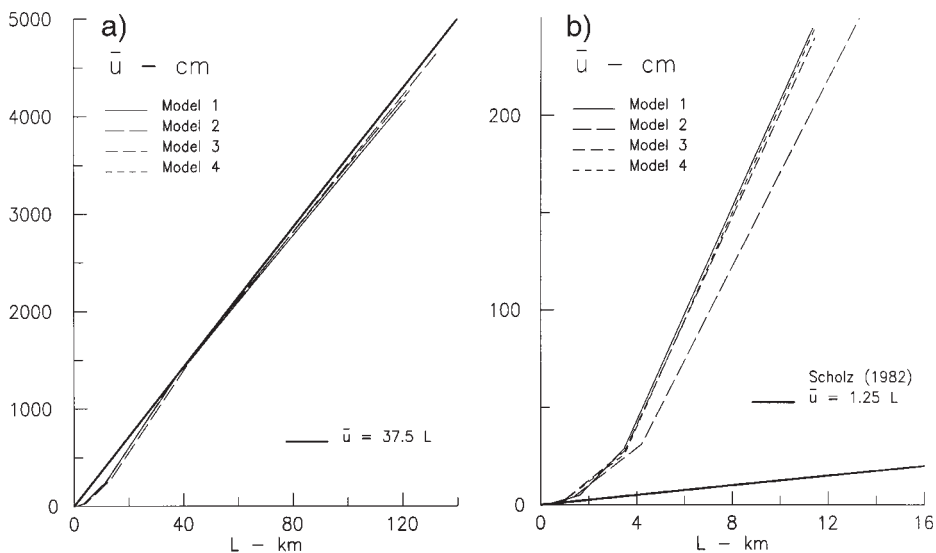

Figure 6. Average dislocation amplitude versus fault length

times smaller α, equal to 1 to 2 for strike slip and thrust earthquakes. For large intra-plate earthquakes, Matsuda et al. (1980) find $\alpha \sim 10$. This »discrepancy« in α, of 2 to 20 times, can be eliminated by recognizing that our rupture length L represents a lower bound (assuming unilateral spreading of the dislocation). For bi-lateral faulting, this »discrepancy« would be reduced to 1 to 10. Furthermore, since some data on L comes from inferences based on
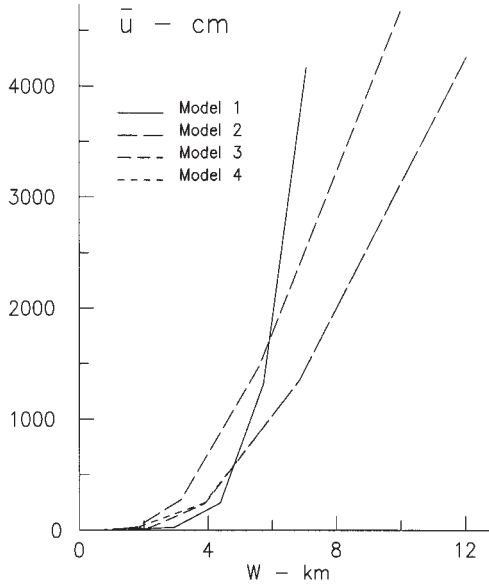
Figure 7. Average dislocation amplitude versus fault width.

the distribution of aftershocks, which often tend to overestimate the initial »dynamic« fault dimensions, it is seen that this discrepancy can further be reduced or eliminated.

By plotting σ versus $(L/W)^{1/2}$, $\log_{10}(L/W)$ and L/W, it was found that only the plot versus $\log_{10}(L/W)$ could be interpreted to lead to a »linear« trend, but with too large scatter to make a convincing case.

To explain the observed high frequency spectral accelerations, the following model (Fig. 8) may be considered. Let x represent length at some representative depth along the seismogenic zone, which is, say, less than 20 km deep (*e.g.* in California). Then the stress in the crust might be distributed as in Fig. 8b. For some strain rate, averaged over the thickness of the seismogenic layer, the stress fluctuations can be a result of large fluctuations in the rigidity, μ, can be caused by some parts of the fault plane being locked while other parts are slipping, can result from stress concentrations near those parts of the fault which remained locked during previous earthquakes, or can be caused by a combination of all of the above. When a »small« earthquake occurs, it will release high stresses over some area (the shaded peak in Fig. 8b and the corresponding small areas in Fig. 8a). If this area of stress concentration is »small« and is surrounded by relatively low stresses, the outcome will be a »single patch« earthquake of magnitude $M < 5$. As this stress drop increases, and as it is released over a progressively larger area, a larger magnitude (*i.e.* moment release) earthquake will occur. As the area of the patch

becomes larger, it may trigger release of stress concentrations on nearby stress peaks.

On the average, it may be expected that an oval fault slip area will be associated with an event as long as its fault dimensions are smaller than W_o, the width of the zone with high stress (Fig. 8a). For the purpose of this discussion, it will be assumed that $W_o \sim$ 3–5 km (for unilateral faulting). As
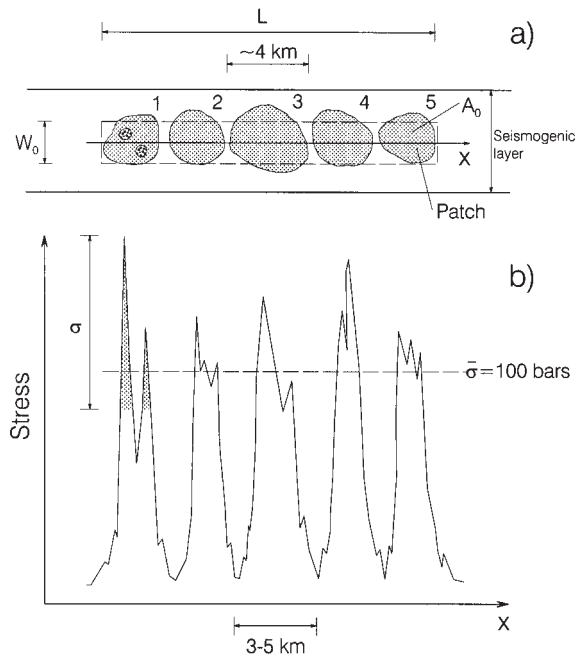

Figure 8. a) Vertical cross-section through shallow crust showing a seismogenic layer and a fault with the »subevents«. b) Distribution of stresses along the fault length L.

larger inertial forces are developed with progressively larger stress drop, accelerating the surrounding medium with progressively larger volume, the first initiating event will grow to the largest possible patch size A_o (here assumed to be ~ 16 km^2) and the excess inertial energy will trigger release of stresses in the area of another, nearby patch, triggering the second event there. Since the growth of the single rupture area (patch) is limited by W_o and by the width of the seismogenic zone, large earthquakes will have to occur on a sequence of patches, more or less extended and propagating along x in one or in two directions. The final fault area $A \sim WL$ will then consist of a number of patches, some smaller and some larger, reflecting the nature of stress oscillations along x, but in no case will a patch size be wider than the

width of the seismogenic zone or much wider than W_o. Obviously, the size of W_o and the width of the seismogenic zone will vary from one tectonic region to another, and will depend on the specific geometrical and physical properties of the area surrounding the fault.

In the above model, the peak spectral acceleration will be associated with the largest of the nearby peaks in the stress pattern, when $M > 5$. In such cases the peaks of stresses plotted in Fig. 8b should be thought of as being low pass filtered below a suitable frequency (say ~10 Hz) to simulate the attenuation effects between the recording station and more distant stress peaks. Since, for simplicity, we used $p = 0.5$ in selecting the $FS(T)_{max}$ amplitudes, the high frequency spectral acceleration should be proportional to the expected value of the largest peaks of the stress patches contributing to the motions recorded. Assuming that the stress indeed fluctuates along x, as suggested by Fig. 8b, then

$$E[\sigma] \sim \overline{\sigma}(\ln N)^{1/2} \qquad (19)$$

where $E[\sigma] \sim FS(T)_{max}$ for $p = 0.5$, $\overline{\sigma}$ is the root mean square of the stress peaks in Fig. 8b, and N is the number of peaks in the stress function after low-pass filtering the stress diagram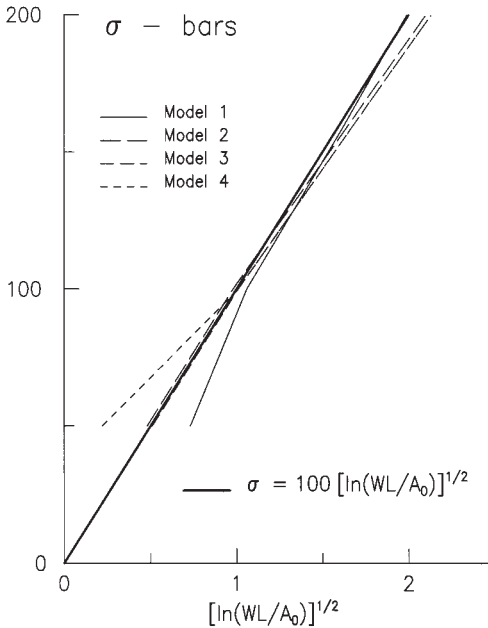 to maintain only the »long period« stress fluctuations. Since $N \sim WL/A_o$, N can be determined if A_o is known or assumed. In this paper it is assumed that, for a single patch, $A_o \sim WL$, but that both $W, L < 4$ km. Using definitions of L and W for the four models in Table 3, for $M = 4, 5, 6, 7$ and 8, the estimates of A_o become ~ 1, 6, 16, 16 and 16 km^2 respectively. For $M > 5$, this gives $E[\sigma] \approx \approx 100(\ln A/A_o)^{1/2}$, as shown in Fig. 9. The remarkably linear growth of $E[\sigma]$ versus $(\ln A/A_o)^{1/2}$ and small scatter of the results predicted for the four extrapolation models suggest that this may be a useful model for further testing and verification. The value of $\overline{\sigma} = 100$ bars is also in good agreement with numerous seismol-

Figure 9. Stress drop, σ, versus $\left[\ln(WL/A_o)\right]^{1/2}$ for extrapolation Models 1 through 4 and for $M \geq 5$.

ogical and strong motion studies (Anderson, 1991) of stress drop inferred from the high frequency spectral amplitudes of recorded body waves.

Within the frequency resolution of the shortest wave length in strong motion data available today (say about 0.5 km for $f < 2$ Hz, associated with the distances at which the records are obtained, with Q, and with the size of geological inhomogeneities along the wave path, rather than with the recording instrumentation), the above suggests that we can think of an earthquake as becoming a multiple event for $M \gtrsim 5$ (in California). Certainly, there is no physical basis to eliminate the possibility of multiple events for $M < 5$ also, but those cannot be identified with the frequency resolution characteristics in the current strong motion data.

For $M < 5$, the situation is different. Then $A < A_o$, and the dynamic stress is associated with stress release on one or two extreme stress peaks. The dislocation stops because the surrounding stress amplitudes are small, because of material barriers, or because of other constraints. Some of these events may have very large dynamic stress drop (Trifunac 1972a, b), but this may occur at very high frequencies, whose amplitudes are »low-pass filtered« by scattering and by attenuation. As the fault dimensions increase, the stress drops further until for a single patch, near say $M = 5$ to 6, it reaches the »troughs« in the stress diagram (Fig. 8b). The average stress drop implied by $\sigma \sim FS(T)_{max}$ (Fig. 2) is then almost same as $\bar{\sigma}$. Beyond $M \sim 6$, in this representation, the stress drop, σ, continues to grow. However, in this model, this is not because the large earthquakes are associated with larger $\bar{\sigma}$, but because A/A_o becomes large and, so, the probability of finding a larger peak increases. Figure 10 summarizes this for $E[\sigma]$ and $\bar{\sigma}$, showing graphically the transition in the nature of this problem near $M = 6$.

Since $\sigma / \mu = \bar{u} / (WC_0^*)$, it is seen that $\bar{\sigma} / \mu = (100 \times 10^6$ dyn/cm$^2) / (1 \times 10^{11}$dyn/cm$^2) = 10^{-3}$. The trend of strain esti-
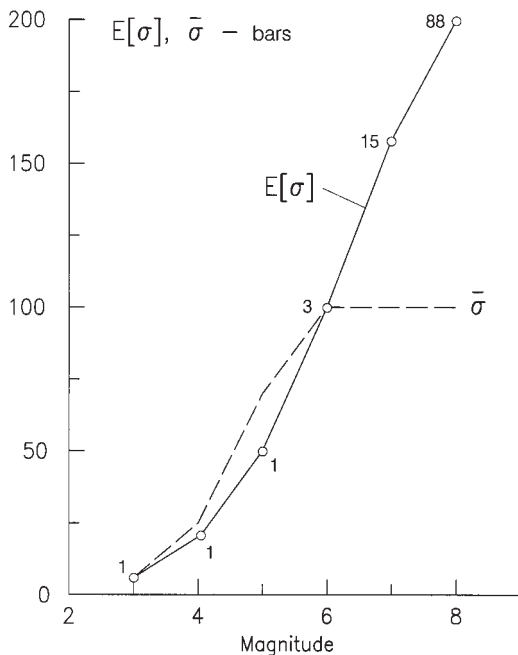

Figure 10. $E[\sigma]$ and stress drop σ versus magnitude. The number of subevents ($N = A/A_o$) in the equation (19) is also shown at magnitudes 3, 4, 5, 6, 7 and 8.

mates ($\overline{u} / WC_0^*$), based on the intermediate and long period estimates gives about 10^{-3} near $M = 6$ ($\overline{\sigma} = 100$ bars), and about 3×10^{-3} near $M = 8$ ($\sigma \sim 200$ bars).

Apparent Stress

The quantity

$$\sigma_a = \eta \frac{\sigma_o + \sigma_1}{2} \tag{20}$$

where σ_o is the stress on the fault before and σ_1 is the stress on the fault surface A, after the earthquake, and η is the seismic efficiency, is called apparent stress (Wyss and Brune, 1968). The seismic energy, E_s, can be represented by

$$E_s = \sigma_a A \overline{u} = \frac{\sigma_a}{\mu} M_o \tag{21}$$

where σ_a is the apparent stress. The Gutenberg and Richter (1956) energy relation $\log_{10} E_s = 1.5 M_s + 11.8$ (M_s – surface wave magnitude) and eq. (21) give

$$\log_{10} \sigma_a = 1.5 M_s + 11.8 - \log_{10} A \overline{u} \tag{22a}$$

or

$$\log_{10} \sigma_a = 1.5 M_s + 11.8 + \log_{10} \mu - \log_{10} M_o . \tag{22b}$$

Equation (20) implies

$$\eta < \frac{2\sigma_a}{\sigma} = \eta_{max} . \tag{23}$$

Figure 11 shows η_{max} versus magnitude. The continuous line represents η_{max}, and was computed for the four extrapolation models which suggest σ_a slowly increasing from 10 bars for $M = 3$ to about 20 bars for $M = 8$ (Trifunac, 1993; 1994b), and using the data from tables in Trifunac (1972a, b).

Frequency of occurrence versus magnitude

In the following, we explore the consequences of our hypothetical model, summarized in eq. (19), on the magnitude-frequency of occurrence relationships in a region. Associating an earthquake event with a patch (an asperity) on the fault surface can be adopted as a causative mechanism to analyze the size (area) and the number of events which can occur on an existing fault. Let $W_{F,i}$ and $L_{F,i}$ represent the widths and the lengths of N_F faults in the region.
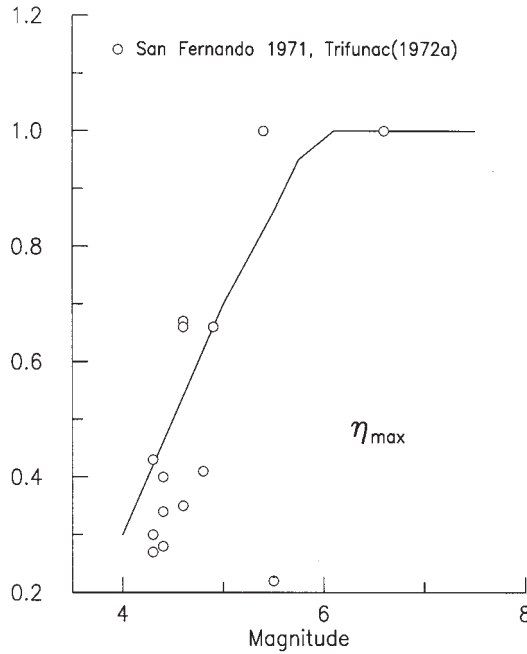
Figure 11. $\eta_{\max}$ versus magnitude

Let W_M and L_M represent the typical length and width of one earthquake event (consisting of one patch for $M < 5$ to 6 or of a group of patches for $M > 6$), determined by the four extrapolation models, for a narrow magnitude interval centered at M ($M \pm \Delta M/2$). Then, if the probability of initiating an event is independent of magnitude, the number of earthquakes, N_M, of magnitude within the interval $M \pm \Delta M/2$ which may occur in the region will be proportional to $\left(\sum_{i=1}^{N_F} W_{F,i} L_{F,i}\right) \big/ (L_M W_M)$. Using the expressions for L and W for our four extrapolation models in Table 3, it follows

$$N_M \sim \frac{\sum_{i=1}^{N_F} W_{F,i} L_{F,i}}{ac} 10^{-(b+d)M}. \tag{24}$$

Since the typical magnitude frequency relationship is of the form $\log_{10} N = \alpha - \beta M$, where N is the number of earthquakes in the magnitude interval $M \pm \Delta M/2$ and α and β are constants, it is seen that $\alpha \sim \log_{10}\left[\left(\sum_{i=1}^{N_F} W_{F,i} L_{F,i}\right) \big/ ac\right]$ and $\beta = b + d$. Equation (24) can be thought of as a »geometrical« constraint due to the fact that the total active fault area in a

region is finite, and only certain number of earthquakes can »fit« within this area.

Empirical estimates of seismicity usually give $0.8 < \beta < 1$. Using the values from Table 3, for $M < M_*$, eq. (24) gives $\beta \sim 1.1$, and for $M > M_*$, it gives $\beta \sim 0.8$, *i.e.* there is a change in the slope of log N versus M relationship. This would imply $\beta \sim 1.1$ for frequency magnitude relationships in subduction zones, for example, or where the thickness of the seismogenic zone does not provide a constraint on one of the fault dimensions, and $\beta \sim 0.5$ to 0.6 for a very shallow seismogenic zone.

For example, for the period between 1900 and present, the Benioff zone only, south of Prince William Sound, and bellow Kenai Peninsula and Kodiak island in Alaska, gives $\beta \sim 0.9$ (for $5 < M < 8$). On the other hand, for shallow faults in the deformed zone behind the trench, and the Castle Mountain Fault north of Cook Inlet, $\beta \sim 0.5$ (for $4 < M < 7$). In Southern California, in the Imperial Valley region, for the period from 1932 to 1971 (Hileman et al., 1973), $\beta \sim 1$ for $3 < M < 5$, and $\beta \sim 0.75$ for $M > 5$.

Another property of the above model is related to the number of stress concentrations (patches) associated with an earthquake event of magnitude M. Assuming that (1) the earthquakes are independent events, and (2) the number of patches, N_M^P relaxed by an earthquake of magnitude M can be computed from eq. (19), the total occurrence rate of earthquakes of magnitude M for the region, N_M^{tot}, will be

$$N_M^{\text{tot}} \sim \frac{\sum_i N_i}{N_M^P} \tag{25}$$

where the summation is over all the seismogenic zones in an area, each with N_i stress concentrations ready to be triggered. From eq. (19), the number of patches (stress concentrations) broken during an earthquake with magnitude M is

$$N_M^P \sim \max\left\{ e^{(E[\sigma(M)]/\overline{\sigma})^2}, 1 \right\} \tag{25a}$$

or

$$N_M^P \sim \max\{ A(M)/A_0, 1 \} \tag{25b}$$

where A_0 is the largest possible patch size, and $A(M)$ is the size of the ruptured area for magnitude M.

For $A(M) < A_0$, or for $E[\sigma(M)] < \overline{\sigma}$, $N_M^P = 1$. Thus $1/N_M^P$ will act as a »low pass filter«, allowing complete throughput for $M < M_p$ and with reduced rate of occurrence for $M > M_p$, where M_p is the magnitude such that $A(M_p) = A_0$, or

for which $E[\sigma(M)] \sim \bar{\sigma}$. The factor, f_{o}, reducing the occurrence rate for $M > M_p$ is

$$f_{\mathrm{o}} = 1/N_M^P. \tag{26}$$

Figure 12 shows N_M^P and Fig. 13 shows f_{o}. It is seen that for $A_{\mathrm{o}} \sim 16$ km^2, and for $M > M_p \sim 5.5$, N_M^P increases from ~ 1, at $M = M_p$, to ~ 100, at $M = 8$.
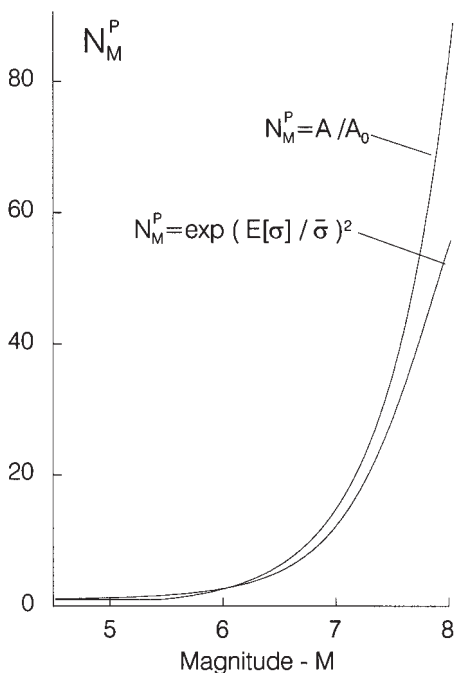
Figure 12. N_M^P (number of patches, subevents) versus magnitude, M.
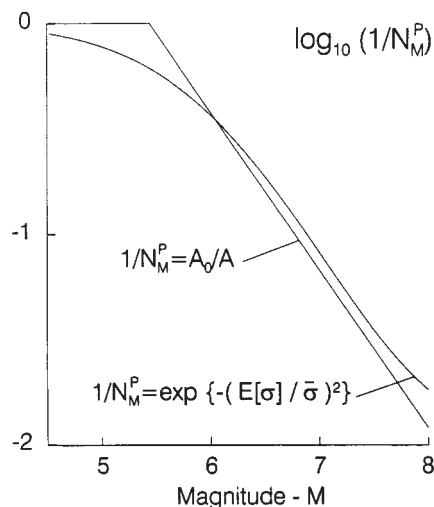
Figure 13. $f_{\mathrm{o}} = 1/N_M^P$ versus M.

Fig. 14 illustrates that three different characteristic shapes of $\log_{10} N$ versus M are possible, assuming that $N \sim N_M/N_M^P$, and depending on whether $W_{\mathrm{o}}^2 > A_{\mathrm{o}}$, $W_{\mathrm{o}}^2 \sim A_{\mathrm{o}}$ or $W_{\mathrm{o}}^2 < A_{\mathrm{o}}$. Detailed analysis of these models is beyond the scope of this paper. Here, we only note that eq. (19) not only fits the trends of the observed Fourier amplitude spectra of strong motion, but may also help in interpretation and understanding of the nature of the variations in the frequency of earthquake occurrence. Further studies of the distributions of W_{o} (width of the zone with high stress concentrations), of the width of the seismogenic zone (*e.g.* in California), and of A_{o} (area of average patch, asperity)
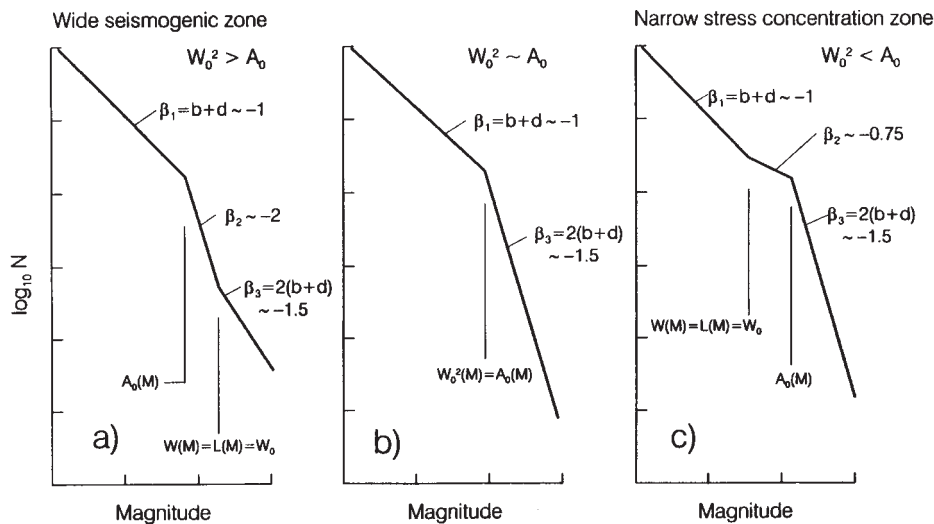
Figure 14. Three hypothetical shapes of $\log_{10} N$ versus M. W_o represents the width of the zone with high stress concentration within the seismogenic zone, and A_o represents the area of an average patch (asperity). (a) Wide zone of high stresses ($W_o^2 > A_o$); (b) $W_o^2 \approx A_o$; (c) Narrow zone of high stresses ($W_o^2 < A_o$).

will show what can be learned from the trends of strong motion amplitudes in the intermediate frequency range and from known geometrical characteristics of seismogenic zones.

Discussion and conclusions

The observed trends of the peak of Fourier amplitude spectrum of strong motion acceleration, $(FS(T))_{max} \sim \sigma$ (σ – stress drop), and of the corresponding estimates of the source dimensions (fault width W and fault length L), along with the average dislocation, $\bar{u}$, the seismic moment, M_o, and the dislocation rise time, T_o, can be interpreted by a population of earthquake events, which, for $M \lesssim 5$, have essentially »circular« faults ($W \sim L$) and are associated with one »patch« (single event, see Figs. 3 and 8). Near $M \approx 5$, the diameter of the patch approaches 3 to 5 km, and is constrained (*e.g.* in California) to grow further by the width of the stress concentration zone, W_o, and by the width of the seismogenic zone. For larger events, the larger fault area is realized by slip on few (M ~ 6) or many such patches (about 100 for M ~ 8). The small and intermediate events can be visualized as »circular« dislocations (see Figs. 3 and 8), but for $M > 7$, our analysis and the strong motion data in California favor long surface faults (strike slip or dip slip, Fig. 3).

The available strong motion data suggests strain drop $\sim 10^{-5}$ for M $\sim$ 3 and strain drop $\sim 10^{-3}$ for M $\sim$ 7. For large events, only $\overline{u}$ appears to be proportional to the fault length (L), but for smaller events it is proportional neither to L nor to W.

For $M > 5$, the expected amplitude of the stress drop, $E[\sigma] \sim (FS(T))_{\max}$, grows linearly with $[\ln(WL / A_{o})]^{1/2}$, where $A_{o} \sim 16$ km^2, and the slope of this linear growth is constant equal to $\overline{\sigma} = 100$ bars, the root mean square of the peaks of stress drop on the fault surface. Our model suggests that $\overline{\sigma}$ grows to ~ 100 bars for $M \sim 6$ and then remains almost constant for $M \gtrsim 6$. Thus, in this interpretation, $E[\sigma]$ continues to grow for $M > 6$, because $[\ln(A / A_{o})]^{1/2}$ grows for large events, while $\overline{\sigma}$ remains close to 100 bars.

References

Anderson, J. G. (1991): Strong motion seismology, *in* Contributions in Seismology, AGU, Washington, D. C.

Brune, J. N. (1970): Tectonic stress and the spectra of seismic shear waves, J. Geophys. Res., **75**, 4997–5009.

Fletcher, J., L. Boatwright, L. Haar, T. Hanks and A. McGarr (1984): Source parameters of aftershcks of the Oroville, California, earthquake, Bull. Seism. Soc. Amer., 74, 1101–1123.

Gutenberg, B. and C. F. Richter 1956): Earthquake magnitude, intensity, energy and acceleration, Bull. Seism. Soc. Amer., **46**, 105–145.

Haskell, N. A. (1969): Elastic displacement in the near field of a propagating fault, Bull. Seism. Soc. Amer., **59**(2), 965–980.

Hileman, J. A., C. R. Allen, and J. M. Nordquist (1973): Seismicity of the Southern California region, Seismological Laboratory, Calif. Inst. of Tech., Pasadena, California.

Izutani, Y. (1981): A statistical model for prediction of quasi-realistic strong ground motion, J. Phys. Earth, **29**, 537–557.

Joyner, W. B. (1984): A scaling law for the spectra of larger earthquakes, Bull. Seism. Soc. Amer., **74**(4), 1167–1188.

Keilis-Borok, V. I. (1959): On estimation of the displacement in an earthquake source and of source dimensions, Annali Geofizica, **12**, 205–214.

Knopoff, L. (1958): Energy release in earthquakes, Geophys. J., **1**, 44–52.

Lee, V. W., M. D. Trifunac and A. Amini (1982): Noise in earthquake accelerograms, J. Eng. Mech. Div., ASCE, **108**, 1121–1129.

Lee, V. W. and M. D. Trifunac (1990): Automatic digitization and processing of accelerograms using PC, Report No. 90-03, Dept. of Civil Eng., Univ. Southern California, Los Angeles, California.

Matsuda, T., H. Yamazaki, T. Nakata, and T. Imaizuni (1980). The surface faults associated with the Rikuu earthquake of 1896, Bull. Earthquake Res. Inst., Univ. of Tokyo, **55**, 795–855.

Papageorgiou, A. S. and K. Aki (1985): Scaling law of far-field spectra based on observed parameters of the specific barrier model, Pageoph, **123**, 353–374.

Richter, C. F. (1958): Elementary seismology, Freeman and Co. S. Francisco.

Scholz, C. H. (1982): Scaling laws for large earthquakes: consequences for physical models, Bull. Seism. Soc. Amer., **72**, 1–14.

Star, A. T. (1928): Slip in a crystal and rupture in a solid due to shear, Cambridge Phil. Society Proc. **24**, 489–500.

Trifunac, M. D. (1971): Zero baseline correction of strong-motion accelerograms, Bull. Seism. Soc. Amer., **61**, 1201–1211.

Trifunac, M. D. (1972a): Stress estimates for San Fernando, California earthquake of February 9, 1971: main event and thirteen aftershocks, Bull. Seism. Soc. Amer., **62**, 721–750.

Trifunac, M. D. (1972b): Tectonic stress and source mechanism of the Imperial Valley, California earthquake of 1940, Bull. Seism. Soc. Amer., **62**, 1283–1302.

Trifunac, M. D. (1972c): A note on correction of strong-motion accelerograms for instrument response, Bull. Seism. Soc. Amer., **62**, 401–409.

Trifunac, M. D. (1973): Analysis of strong earthquake ground motion for prediction of response spectra, Earthquake Eng. and Struct. Dynam., **2**(1), 59–69.

Trifunac, M. D. (1974): A three-dimensional dislocation model for the San Fernando, California, earthquake of February 9, 1971, Bull. Seism. Soc. Amer., **64**, 149–172.

Trifunac, M. D. (1976): Preliminary empirical model for scaling Fourier amplitude spectra of strong ground acceleration in terms of earthquake magnitude, source to station distance and recording site conditions, Bull. Seism. Soc. Amer., **66**, 1343–1373.

Trifunac, M. D. (1989a): Dependence of Fourier spectrum amplitudes of recorded strong earthquake accelerations on magnitude, local soil conditions and on depth of sediments, Earthquake Eng. and Struct. Dynam., **18**, 999–1016.

Trifunac, M. D. (1989b): Empirical scaling of Fourier spectrum amplitudes of recorded strong earthquake accelerations in terms of magnitude and local soil and geologic conditions, Earthquake Eng. and Eng. Vibration, **9**(2), 23–44.

Trifunac, M. D. (1990): How to model amplification of strong earthquake motions by local soil and geologic site conditions, Earthquake Eng. and Struct. Dynam., **19**(6), 833–846.

Trifunac, M. D. (1991): M_L^{SM}, Soil Dynam. and Earthquake Eng., **10**(1), 17–25.

Trifunac, M. D. (1993): Long period Fourier amplitude spectra of strong motion acceleration, Soil Dynam. and earthquake Eng., **12**(6), 363–382.

Trifunac, M. D. (1994a). Q and high frequency strong motion spectra, Soil Dynam. and Earthquake Eng., **13**(3), 149–161.

Trifunac, M. D. (1994b): Similarity of strong motion earthquakes in California, European Earthquake Eng., **VIII**, n. 1., 38–48.

Trifunac, M. D. (1995a). Pseudo relative velocity spectra of earthquake ground motion at long periods, Soil Dynam. and Earthquake Eng., **14**(5), 331–346.

Trifunac, M. D. (1995b): Pseudo relative velocity spectra of earthquake ground motion at high frequencies, Earthquake Eng. and Struct. Dynam., **24**(8), 1113–1130.

Trifunac, M. D. and D. E. Hudson (1970): Laboratory evaluation and instrument corrections of strong motion accelerographs, Report EERL 70-04, Earthquake Eng. Res. Lab., Calif. Inst. of Tech., Pasadena.

Trifunac, M. D. and V. W. Lee (1985): Preliminary empirical model for scaling Fourier amplitude spectra of strong ground acceleration in terms of earthquake magnitude source to station distance, site intensity and recording site conditions, Report No. 85-03, Dept. of Civil Eng., Univ. of Southern Calif., Los Angeles, California.

Trifunac, M. D. and V. W. Lee (1987): Direct empirical scaling of response spectral amplitudes from various site and earthquake parameters, Report NUREG/CR-4903, U. S. Nuclear Regulatory Commission, **1**.

Trifunac, M. D. and V. W. Lee (1989): Empirical models for scaling Fourier amplitude spectra of strong ground acceleration in terms of earthquake magnitude, source to station distance, site intensity and recording site conditions, Soil Dynam. and Earthquake Eng., **8**(3), 110–125.

Trifunac, M. D. and V. W. Lee (1990): Frequency dependent attenuation of strong earthquake ground motion, Soil Dynam. and Earthquake Eng., **9**(1), 3–15.

Wyss, M. and J. N. Brune (1968): Seismic moment, stress and source dimensions for Earthquakes in California-Nevada Region, J. Geophys. Res., **73**, 4681–4694.

SAŽETAK

Napetosti i središnji interval frekvencija pri akceleraciji tla za jakih potresa

M. D. Trifunac

Ekstremi izglađenih Fourierovih spektara, $(FS(T))_{max}$, akcelerograma jakih potresa u Kaliforniji modelirani su dimenzionalnom analizom. U tom modelu spektri amplitude proporcionalni su sa: (1) $\bar{\sigma}$ – r.m.s. iznosu amplitude vršnih napetosti u područjima visoke napetosti na rasjednoj plohi i (2) $(\log N)^{1/2}$ – gdje je N broj takvih područja. Jednostavni modeli rasjeda s jednim područjem visoke koncentracije napetosti prikladni su za opis potresa s magnitudom $M \lesssim 5$, dok za veće magnitude u obzir treba uzeti više takvih područja ($N \sim 10$ oko $M = 7$ i $N \sim 100$ za $M \sim 8$). r.m.s. iznos parametra $\bar{\sigma}$ čini se da raste s magnitudom za $M \lesssim 6$, dok je za veće magnitude približno konstantan i iznosi oko 100 bara. Za $M > 6$, $(FS(T))_{max}$ raste s magnitudom zbog velikog broja područja visoke napetosti koja doprinose spektru ($N \sim 100$ za $M = 8$), a ne zbog povećanja $\bar{\sigma}$.

Author's address: M. D. Tifunac, University of Southern California, Department of Civil Engineering, Kaprielian Hall 216 D, Los Angeles, California, 90089-2531, USA